ACS APPLIED MATERIALS & INTERFACES

www.acsami.org

Research Article

Thermal-Driven Optimization of the Strong Metal–Support Interaction of a Platinum–Manganese Oxide Octahedral Molecular Sieve to Promote Toluene Oxidation: Effect of the Interface $Pt^{2+}–O_v–Mn^{\delta+}$

Lixin Zhang, Zhengxuan Zhu, Wei Tan, Jiawei Ji, Yandi Cai, Qing Tong, Yan Xiong, Haiqin Wan,* and Lin Dong

Cite This: *ACS Appl. Mater. Interfaces* 2022, 14, 56790–56800

Read Online

ACCESS | Metrics & More | Article Recommendations | Supporting Information

ABSTRACT: Strong metal–support interactions (SMSIs) have a significant effect on the performance of supported noble-metal catalysts for volatile organic compound (VOC) elimination. Herein, the strength of the SMSI of Pt/OMS-2 between Pt and the OMS-2 support is regulated by simply changing calcination temperatures, and the catalyst calcined at 300 °C (Pt/OMS-2-300) performs the best in the catalytic combustion of toluene. Through systematic structural characterizations, it is revealed that much more $Pt^{2+}–O_v–Mn^{\delta+}$ species are formed in Pt/OMS-2-300, which can help facilitate the generation of more reactive oxygen species and promote lattice oxygen mobility. Moreover, the results of in situ DRIFTS experiments further confirm that abundant $Pt^{2+}–O_v–Mn^{\delta+}$ species at the Pt–MnO_2 interface on Pt/OMS-2-300 can better enhance the adsorption and activation of toluene, thus boosting the catalytic performance in toluene combustion. This newly developed strategy of thermal-driven regulation of the SMSI provides a novel perspective for constructing highly efficient catalysts for VOC emission control.

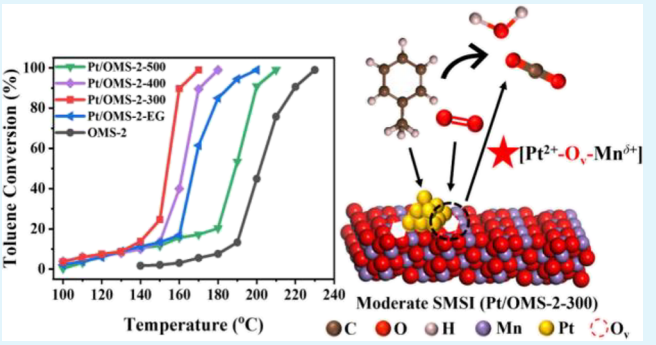

KEYWORDS: *Pt/OMS-2, strong metal–support interaction, thermal-driven, reactive oxygen species, toluene oxidation*

1. INTRODUCTION

Volatile organic compounds (VOCs) not only are harmful to human health but also are important precursors of $PM_{2.5}$ and O_3, causing serious environmental problems. To realize the effective control of VOC emissions, increasingly stringent laws and regulations on VOC emissions are enforced.[1,2] Toluene, as one of the typical VOCs, is widely used as a solvent in industrial processes such as those of paint, adhesive, rubber, and leather as well as an additive in petroleum and gasoline, which has wide discharge and high toxicity.[3] Therefore, toluene is usually used as a model pollutant in the study of VOC elimination technologies. Among all kinds of control technologies, catalytic oxidation has become the most promising control technology because of its low energy consumption, high treatment efficiency, and absence of secondary pollution.[3−5]

Various catalysts, such as transition-metal oxides and supported noble metals, have been developed for the oxidation of VOCs.[6−8] Supported Pt-based catalysts have received wide attention due to their outstanding low-temperature activity.[9−11] Generally, fine-tuning the strong metal–support interaction (SMSI) is the most considered strategy in the design of supported Pt-based catalysts, which could significantly alter the activity and stability of the catalysts.[12] In 1978, Tauster et al. first proposed the concept of SMSIs, which well explained the difference of H_2 adsorption and desorption on precious-metal surfaces, such as Pt, Pd, and Rh.[13] Since then, the SMSI has been widely reported as a universal phenomenon in the field of heterogeneous catalysis.[14−16] SMSIs can hinder the growth of small metal nanoparticles, optimize the bonding structure and electron transfer, and thus enhance the catalytic performance. However, some studies have shown that too strong interactions may limit the catalytic reaction and weaken the catalytic activity. Miao and Deng found that excessively strong metal–support interactions were not conducive to O_2 adsorption.[17] Pereira-Hernández et al. weakened the strong

Received: September 20, 2022
Accepted: December 5, 2022
Published: December 16, 2022

interaction between Pt single atoms and the CeO_2 support by CO reduction, resulting in the generation of highly active Pt clusters and fruitful oxygen defects at the Pt−CeO_2 interface, which could facilitate the catalytic oxidation of CO.[18] Therefore, rational regulation of the interaction between metal and support is the key point to design the highly efficient catalyst.

The manganese oxide octahedral molecular sieve (OMS-2) belongs to the α-MnO_2 phase and possesses a one-dimensional tunnel structure consisting of 2 × 2-edged shared MnO_6 octahedral chains.[19] Because of the existence of variable manganese ions, OMS-2 exhibits superior redox properties. Several studies have explored the effect of the interaction between Pt and MnO_x on toluene oxidation by changing the different crystal types and morphologies of MnO_x.[20,21] Mo et al.[21] found that the catalytic behaviors of Pt/MnO_2 closely depended on the crystal structures of MnO_2, which related with the SMSI between Pt NPs and MnO_2. They observed that Pt/α-MnO_2 exhibited the best catalytic activity for total toluene oxidation (T_{90} = 170 °C) among α-, β-, γ-, and hollow-MnO_2, and the characterization results indicated that the SMSI between Pt NPs and α-MnO_2 resulted in improved low-temperature reducibility and mobility of oxygen species by optimizing surface chemical states and weakening surface Mn−O bonds.[21] Moreover, calcination conditions were also reported to have an appreciable effect on the catalytic performance in terms of oxygen-vacancy levels.[22,23] Considering the special role of oxygen vacancies, it can adsorb and activate oxygen to produce more reactive oxygen species, which cannot be neglected.[24,25] However, few studies have demonstrated how SMSI changes oxygen species and affects the deep oxidation of toluene, which is worth further study.

Based on this, a new strategy of tuning the strength of the SMSI between Pt species and OMS-2 support by controlling the calcination temperature was developed, which could help maximize the toluene combustion activity on Pt/OMS-2 catalysts. To further reveal the effect of the calcination temperature on the strength of the SMSI and establish a structure−activity relationship on Pt/OMS-2, a series of characterizations were carried out.

2. EXPERIMENTAL SECTION

2.1. Materials. Potassium permanganate ($KMnO_4$) and acetic acid were purchased from Sinopharm Chemical Reagent Co., Ltd. (China). Manganese acetate tetrahydrate ($MnAc_2{\cdot}4H_2O$) was purchased from Nanjing Chemical Reagent Co., Ltd. (China). Chloroplatinic acid hexahydrate ($H_2PtCl_6{\cdot}6H_2O$) and polyvinyl pyrrolidone (PVP) were obtained from Aladdin. Ethylene glycol was obtained from Alfa Aesar. All chemical reagents were of analytical grade and used without further purification.

2.2. Preparation of Catalysts. The Pt NPs were synthesized by a microwave-assisted ethylene glycol (EG) reduction method.[26] First, 15 mL of EG and 100 mg of PVP were mixed and put into a 50 mL three-necked flask, which was placed in a CEM-MARS-5 microwave reactor. When the temperature was stable at 150 °C, 1.2 mL of $H_2PtCl_6{\cdot}6H_2O$ (0.02 M) and 1 mL of NaOH (0.25 M) were injected to the three-necked flask. The mixture was heated for another 30 min before the reaction was stopped by cooling the flask in an ice-water bath. Then, the product was washed with acetone, ethanol, and n-hexane several times to remove the PVP. The Pt NPs were dispersed and preserved in ethanol solution.

The OMS-2 materials were prepared with a conventional hydrothermal method. $MnAc_2{\cdot}4H_2O$ (3.668 g) was dissolved in 40 mL of water. Then, 2.5 mL of acetic acid was added in order to keep an acidic environment. Afterward, $KMnO_4$ (2.168 g) was dissolved in 35 mL of water and added in the above mixture dropwise under stirring. Subsequently, the mixed solution was transferred to a Teflon-lined autoclave and maintained at 100 °C for 24 h and then cooled to room temperature. The as-obtained precipitates were washed with deionized water several times. Finally, the dark precipitates were dried at 100 °C for 12 h and calcined at 400 °C for 4 h with a ramping rate of 5 °C·min^{-1} to obtain OMS-2. To deposit Pt NPs onto the OMS-2 support, an ethanol solution of Pt NPs was dropped into an ethanol solution of OMS-2. After stirring for 4 h, the product was evaporated through a water bath (80 °C) and then dried at 100 °C for 4 h. After grinding, the product was denoted as Pt/OMS-2-EG. Then, Pt/OMS-2-EG was calcined at 300, 400, or 500 °C for 2 h. The obtained sample was denoted as Pt/OMS-2-x (x represented the calcination temperature). The actual Pt loading in the samples measured by ICP was 0.35%.

2.3. Catalyst Characterization. Physicochemical properties of the as-prepared samples were characterized using the following techniques, including inductively coupled plasma atomic emission spectroscopy (ICP−AES), X-ray diffraction (XRD), N_2 adsorption−desorption (BET), transmission electron microscopy (TEM) and high-resolution TEM (HRTEM), high-angle annular dark-field scanning transmission electron microscopy (HAADF−STEM) and element mapping, energy-dispersive spectroscopy (EDS), CO pulse chemisorption, X-ray photoelectron spectroscopy (XPS), oxygen temperature-programmed desorption (O_2-TPD), toluene temperature-programmed desorption (toluene-TPD), hydrogen temperature-programmed reduction (H_2-TPR), thermogravimetry−mass spectrometry (TG-MS), and in situ diffuse reflectance infrared Fourier transform spectroscopy (in situ DRIFTS). The detailed procedures are described in the Supporting Information.

2.4. Catalytic Activity Test. The catalytic performance of Pt/OMS-2 for toluene was tested in a continuous flow fixed-bed microreactor with a WHSV of 30,000 mL·g^{-1}·h^{-1}. An amount of 100 mg of the catalyst (20−40 mesh) was loaded into a quartz tube. After heating to 100 °C, 1000 ppm toluene was introduced into the pure air flow (N_2/O_2 = 4:1; total flow rate = 50 mL·min^{-1}). Each testing temperature point was maintained for 30 min, and the reaction products were detected and analyzed by a flame ionization detector (FID) and thermal conductivity detector (TCD), and the average value of three times was calculated. To study the effect of water vapor on catalytic activity, 5 vol % H_2O was introduced into feed vapor through a water saturator. Toluene conversion ($X_{toluene}$, %) was calculated using the following formula:

$$X_{toluene}\ (\%) = \frac{C_{in} - C_{out}}{C_{in}} \times 100\% \quad (1)$$

C_{in} and C_{out} are toluene concentrations at the inlet and outlet of the feed flow, respectively.

The CO_2 yield (Y_{CO2}, %) was calculated using the following equation:

$$Y_{CO_2}\ (\%) = \frac{C_{CO_2}}{7C_{in}} \times 100\% \quad (2)$$

where C_{CO2} represents the CO_2 concentration in the outlet gas.

To calculate the turnover frequency (TOF) and the apparent activation energy (E_a), the catalyst mass was reduced to 50 mg. TOF and E_a were obtained by controlling the reaction temperature to ensure a toluene conversion rate below 10%. TOF was calculated as follows:

$$TOF_{Pt}\ (s^{-1}) = X_{toluene} \times V_{toluene} \times \frac{M_{Pt}}{m_{cat}X_{Pt}D_{Pt}} \quad (3)$$

where $X_{toluene}$ represents the toluene conversion rate at corresponding temperatures, $V_{toluene}$ is the toluene flow rate (mol·s^{-1}), M_{Pt} is the molar mass of Pt, m_{cat} is the amount of the catalyst, X_{Pt} is the mass fraction of Pt in the catalyst, and D_{Pt} is the dispersion of Pt.

E_a was calculated using the Arrhenius equation as follows:

https://doi.org/10.1021/acsami.2c16923
ACS Appl. Mater. Interfaces 2022, 14, 56790−56800

$$\ln k = \ln A - \frac{E_a}{RT} \quad (4)$$

where k is the reaction rate (mol·s^{-1}), E_a is the apparent activation energy (kJ·mol^{-1}), and A is the pre-exponential factor.

3. RESULTS AND DISCUSSION

3.1. Structure and Morphology of Catalysts. The crystal phase and crystallinity of the samples were determined by XRD. As shown in Figure 1, all samples showed diffraction peaks at 2θ of 12.8, 18.1, 28.8, 37.5, 41.9, 49.9, 60.3, and 65.1°, corresponding to the (110), (200), (310), (211), (301), (411), (521), and (002) planes of the OMS-2 phase (JCPDS PDF no. 44-0141).[21] No crystal phases of Pt were observed, implying that Pt species were highly dispersed on the OMS-2 surface. The N_2 adsorption−desorption isotherms and BJH pore size distribution curves of all samples are shown in Figure S1, and all catalysts showed the type IV isotherms with H_3 hysteresis loops, indicating that there were some piled mesopores in the catalysts. After loading Pt, the specific surface areas, pore volumes, and average pore diameters of the catalysts showed limited changes (Table S1).

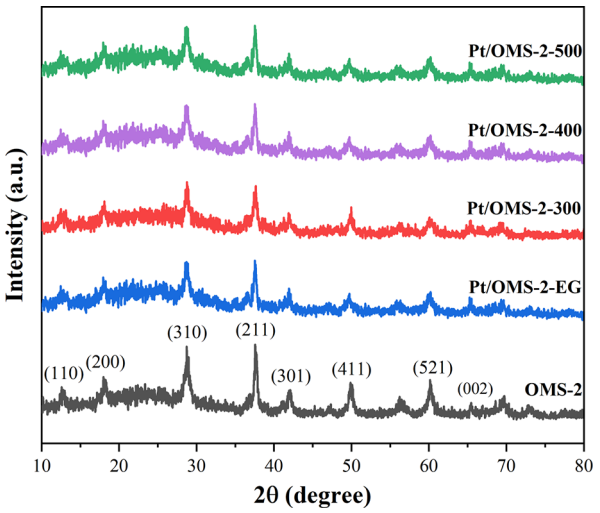

Figure 1. XRD patterns of various Pt/OMS-2 and OMS-2 samples.

In order to investigate the morphology of the catalysts, TEM and HRTEM images of all the samples were collected, and the particle size distribution of Pt was analyzed (Figure 2 and Figure S2). Figure S2 shows that the pure OMS-2 sample presented well-defined one-dimensional uniform nanorods with a diameter of 10−20 nm, and the length of a single nanorod ranged from a few tens to hundreds of nanometers. After the deposition of Pt, all Pt/OMS-2-x samples showed a good rod-shaped morphology, and Pt NPs were well dispersed on the OMS-2 surface without further aggregation, which was consistent with XRD and BET results. As shown in Figure 2e−h, the lattice fringes with a d spacing of 0.30 and 0.49 nm were indexed to the (310) and (200) planes of OMS-2, respectively. The lattice fringes of 0.23 nm corresponding to the (111) plane of Pt NPs was also observed.[15] Additionally, the average particle sizes and their distributions were obtained based on the measurement of at least 200 individual particles. The mean particle sizes of Pt species for Pt/OMS-2-EG, Pt/OMS-2-300,

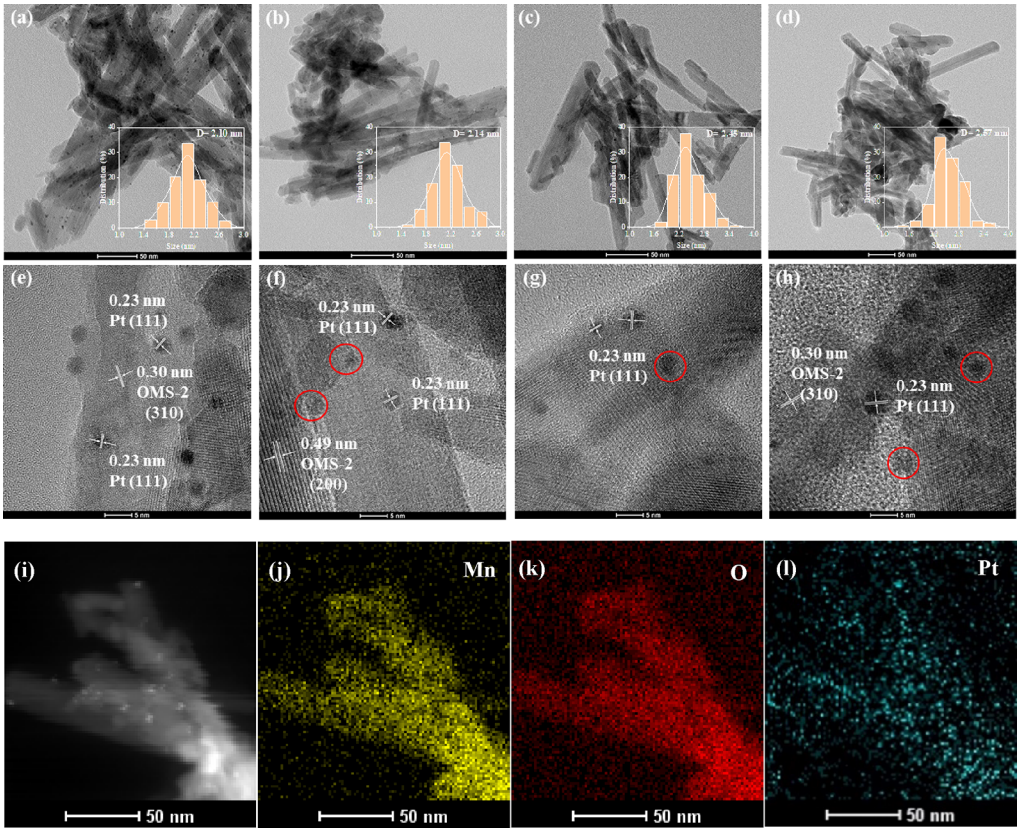

Figure 2. TEM and HRTEM images of (a, e) Pt/OMS-2-EG, (b, f) Pt/OMS-2-300, (c, g) Pt/OMS-2-400, and (d, h) Pt/OMS-2-500, and the bar chart is the corresponding particle size distribution of Pt. (i) HAADF-STEM images and (j−l) EDS elemental mapping images of Pt/OMS-2-300.

https://doi.org/10.1021/acsami.2c16923
ACS Appl. Mater. Interfaces 2022, 14, 56790−56800

Pt/OMS-2-400, and Pt/OMS-2-500 were 2.10, 2.14, 2.45, and 2.57 nm, respectively. With the increasing calcination temperature, the particle size of Pt tended to become larger, and such a slight increase in the average diameter of Pt particles might be due to the slight agglomeration of Pt or the transformation of spheres to hemispheres during calcination.[27] In addition, for the Pt/OMS-2-EG catalyst, the Pt nanoparticles were deposited on the surface of the OMS-2 support without close interactions (Figure 2e). However, as visualized in Figure 2f,g,h, the Pt nanoparticles were deposited on the OMS-2 support via an intimate interfacial contact in the Pt/OMS-2-*x* catalysts (red circle), indicating the generation of a strong interaction between the Pt nanoparticles and OMS-2.[28] Furthermore, from EDS-mapping images (Figure 2j–l), it could be seen that the dispersion of Pt was fine on the surface of OMS-2.

Table 1. Noble-Metal Particle Size and Catalytic Performance of the Catalysts

catalyst	Pt particle size (nm)	D_{CO} (%)[a]	T_{90} (°C)[b]	TOF (s^{-1})	E_a ($kJ \cdot mol^{-1}$)
OMS-2			220		74.16
Pt/OMS-2-EG	2.10	59.4	186	6.6×10^{-3}	47.06
Pt/OMS-2-300	2.14	58.5	162	8.0×10^{-3}	22.70
Pt/OMS-2-400	2.45	39.2	173	7.5×10^{-3}	32.14
Pt/OMS-2-500	2.57	35.5	200	3.9×10^{-3}	50.99

[a]The dispersion of Pt was calculated by CO pulse chemisorption. [b]T_{90} was the temperature at which a toluene conversion of 90%.

3.2. Relationship between the Strength of the SMSI and Calcination Temperature. In order to investigate the trend of the interaction between Pt and OMS-2 with increasing the calcination temperature, XPS measurements of the prepared samples were collected. The Mn $2p_{3/2}$ XPS of all samples is shown in Figure 3a. The three main peaks near 640.0–640.6, 641.5–642.0, and 643.0–643.5 eV were attributed to Mn^{2+}, Mn^{3+}, and Mn^{4+}, respectively.[29] It could be found that the three kinds of Mn species existed in all samples, but the ratio of each Mn species was different. According to the fitting results, the molar ratio of Mn with a lower valence (Mn^{2+} + Mn^{3+}) to Mn^{4+} ((Mn^{2+} + Mn^{3+})/Mn^{4+}) increased from 1.97 to 2.11–2.83 after loading of Pt NPs, indicating that the deposition of Pt NPs could facilitate the formation of Mn species with a lower valence. Moreover, it was interesting to observe that the concentration of low-valence Mn on Pt/OMS-2 first increased after the calcination at 300 °C and then decreased with the temperature further increased. The higher concentration of surface low-valence Mn on Pt/OMS-2-300 also suggested the formation of more surface oxygen vacancies, which always formed accompanying the low-valence Mn species.[29] Raman spectroscopy also proved the formation of oxygen vacancies (Figure S3). With the introduction of Pt, the lattice vibration mode of Mn–O corresponding to 570 and 630 cm^{-1} became weaker and broader, suggesting that the introduction of Pt could induce the lattice distortion and generation of oxygen defects on OMS-2.[30,31] The average oxidation state (AOS) of Mn was calculated according to ΔEs (the distance between the binding energy of two peaks) of the Mn 3s spectrum (Figure 3b and Table 2), which further verified the generation of more surface low-valence Mn species on Pt/OMS-2 samples compared with OMS-2.[3,32] It was worth noting that the Mn 2p spectra of Pt/OMS-2 samples move toward higher binding energies with the increase of treatment temperature, indicating the enhancement of strong metal–support interactions.[15]

Three peaks could be observed on O 1s XPS for all samples, which could be assigned to surface lattices oxygen (ca. 529.2 eV, marked as O_{latt}), surface chemisorbed oxygen species (ca. 530.8 eV, marked as O_{ads}), and oxygen species in surface hydroxyl groups (ca. 532.5 eV, OH), respectively.[33] The O_{ads}/O_{total} molar ratios followed the order of Pt/OMS-2-300 (17.2%) > Pt/OMS-2-400 (16.1%) > Pt/OMS-2-EG (15.8%) > Pt/OMS-2-500 (15.3%) > OMS-2 (14.1%), which showed the same order with the low valence Mn species (Figure 3c), well supporting the viewpoint that the higher concentration of surface low-valence Mn species could help the generation of more oxygen vacancies on Pt/OMS-2-*x*. Furthermore, it has been reported that the electrophilic O_{ads} species played a vital role in the combustion of organics.[33] Therefore, high concentrations of adsorbed oxygen in Pt/OMS-2-300 might favor the catalytic combustion of toluene.

As shown in Figure 3d, Pt 4f XPS spectra for Pt/OMS-2-EG and Pt/OMS-2-*x* were decomposed into six components at BE = 71.2 and 74.7 eV, 72.5 and 75.8 eV, and 74.1 and 77.5 eV, which were attributed to the $4f_{7/2}$ and $4f_{5/2}$ orbitals of Pt^0, Pt^{2+}, and Pt^{4+}, respectively.[34] As listed in Table 2, it could be found that higher concentrations of $Pt^{\delta+}$ (Pt^{2+} and Pt^{4+}) species were formed on Pt/OMS-2 catalysts as the calcination temperature increased from 100 to 500 °C, which could be related to the formation of the stronger SMSI.[35] According to the results of XPS, the average chemical state of Pt was also calculated.[36] It is worth noting that Pt/OMS-2-300 possessed the highest content of Pt^{2+} and the average chemical state of Pt was around 2.26, indicating that moderate strength of SMSIs generated the most intermediate valence Pt. Combined with the above XPS results of Mn and O, it could be concluded that Pt/OMS-2-300 had the highest content of low-valence Mn species, (Mn^{2+} and Mn^{3+}, denoted as $Mn^{\delta+}$), oxygen vacancies (O_v), and Pt^{2+} species compared to other Pt/OMS-2-*x*. It was reasonable to propose that the most surface synergetic oxygen vacancies (SSOV; Pt^{2+}–O_v–$Mn^{\delta+}$) were formed at the interface of Pt/OMS-2-300.[37]

The O_2-TPD experiment was carried out to study the relationship between the strength of the SMSI and oxygen species of Pt/OMS-2 (Figure 4a). The desorption peak at 100–120 °C was attributed to surface adsorption oxygen (O_{ads}), which could rapidly participate in the combustion of toluene owing to its weakly bound to the surfaces.[38] The desorption peak at 300–450 °C was attributed to surface lattice oxygen (O_{latt}), which arose from the breakage of Mn–O and Pt–O–Mn, and the desorption peak at 500–750 °C was attributed to bulk lattice oxygen.[39] For OMS-2, the mobility of surface lattice oxygen was relatively poor. After loading Pt and thermal treatment, the desorption peak of O_{latt} moved to a lower temperature, indicating the easier migration of oxygen resulting from the formation of SMSIs in the Pt–MnO_2 interface. Compared to other catalysts, the pattern of Pt/OMS-2-300 showed much more O_{ads} species, a lower desorption temperature of the surface lattice oxygen, and a weaker peak intensity of the bulk lattice oxygen, which indicated more abundant oxygen migration from the bulk phase to the surface or subsurface as the sample was calcined at 300 °C.[40] For Pt/OMS-2-EG, a weak SMSI meant less breakage of Mn–O and thus gave rise to low oxygen mobility, while for Pt/OMS-2-500, excessive SMSIs would stabilize the

https://doi.org/10.1021/acsami.2c16923
ACS Appl. Mater. Interfaces 2022, 14, 56790–56800

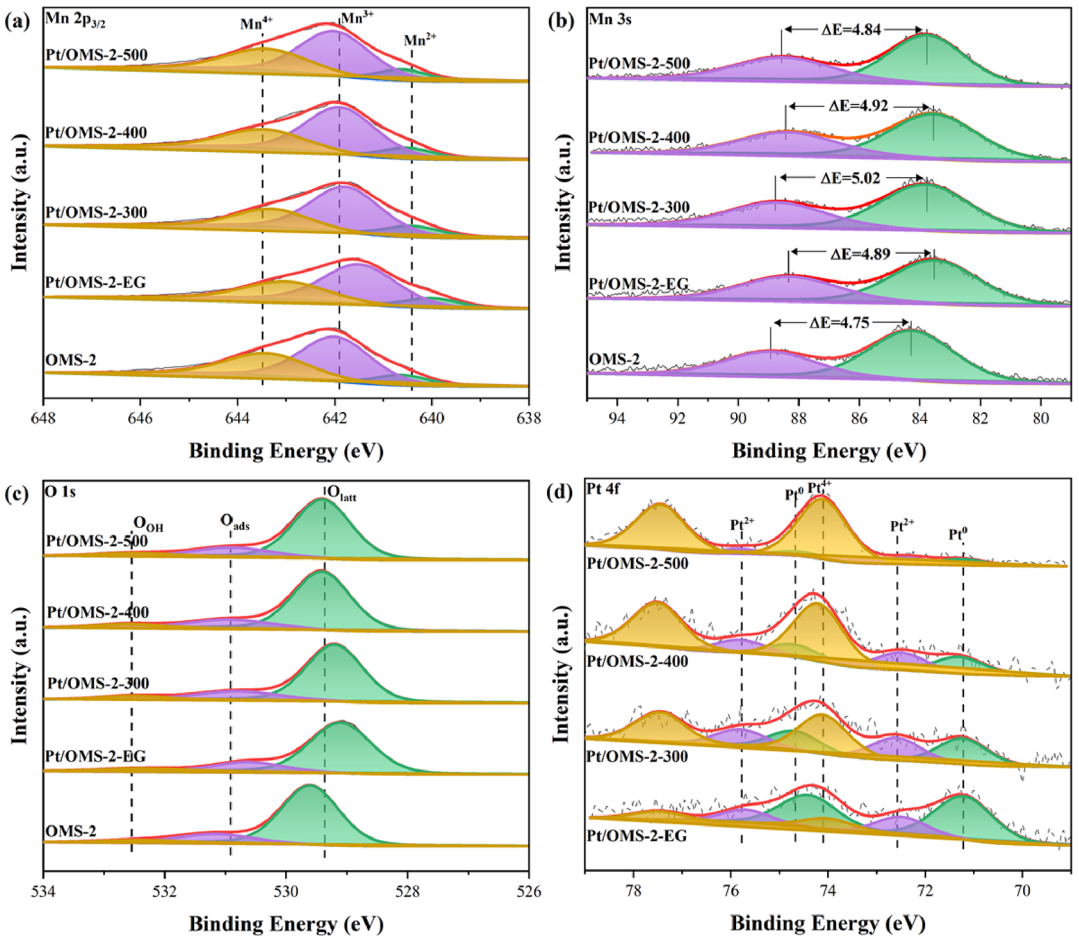

Figure 3. (a) Mn $2p_{3/2}$, (b) Mn 3 s, (c) O 1s, and (d) Pt 4f XPS spectra for as-prepared Pt-based samples.

Table 2. XPS Results of the Catalysts

catalyst	OMS-2	Pt/OMS-2-EG	Pt/OMS-2-300	Pt/OMS-2-400	Pt/OMS-2-500
Pt^0/Pt_{total}		0.65	0.31	0.18	0.08
Pt^{2+}/Pt_{total}		0.22	0.25	0.19	0.08
Pt^{4+}/Pt_{total}		0.13	0.44	0.63	0.84
Pt average valence state[a]		0.96	2.26	2.90	3.52
$(Mn^{2+} + Mn^{3+})/Mn^{4+}$	1.97	2.30	2.83	2.45	2.11
O_{ads}/O_{total} (%)	14.1	15.8	17.2	16.1	15.3
AOS[b]	3.61	3.45	3.30	3.42	3.51

[a]Average valence state was calculated by the XPS results. [b]AOS = 8.956 − 1.126ΔE_s (eV).

lattice oxygen and suppress the activation and migration of oxygen species. This implied that Pt/OMS-2 treated at 300 °C led to a moderate SMSI, which could enhance lattice oxygen migration and generate more active oxygen species due to the SSOV of $Pt^{2+}-O_v-Mn^{\delta+}$.

Toluene TPD was carried out to detect the adsorption and desorption of toluene over Pt/OMS-2-*x*. The intensity of the desorption peak showed the adsorption capacity for toluene in the catalysts.[39] As shown in Figure 4b, both Pt/OMS-2-300 and Pt/OMS-2-500 exhibited a higher toluene adsorption capacity and a lower toluene desorption temperature than Pt/OMS-2-EG, which indicated that the formation of an SMSI between Pt and OMS-2 could enhance toluene adsorption ability. Compared with Pt/OMS-2-500, the major desorption peak of Pt/OMS-2-300 was detected at a lower temperature and the strength of the desorption peak was weaker.[41] It should be noted that, although a high coverage of reactants was necessary to enhance the catalytic reaction, excessive adsorption of toluene at the Pt site might cause catalyst poisoning. Combining with the O_2-TPD and XPS results, it could be reasonably deduced that toluene adsorption was not responsible for catalytic activity and surface synergistic oxygen vacancies might dominate the combustion of toluene.

The H_2-TPR experiment was conducted to further investigate the relationship between the reduction properties and the strength of the SMSI of Pt/OMS-2 samples. Only one reduction peak of OMS-2 was observed at 338 °C, which was attributed to multi-step reduction of $Mn^{4+} \rightarrow Mn^{3+} \rightarrow Mn^{2+}$.[42] After depositing Pt NPs to the surface of OMS-2, some interesting results were determined as shown in Figure 5a. For Pt/OMS-2 samples, besides the peak at 290−340 °C corresponding to the reduction of OMS-2, a new reduction

https://doi.org/10.1021/acsami.2c16923
ACS Appl. Mater. Interfaces 2022, 14, 56790−56800

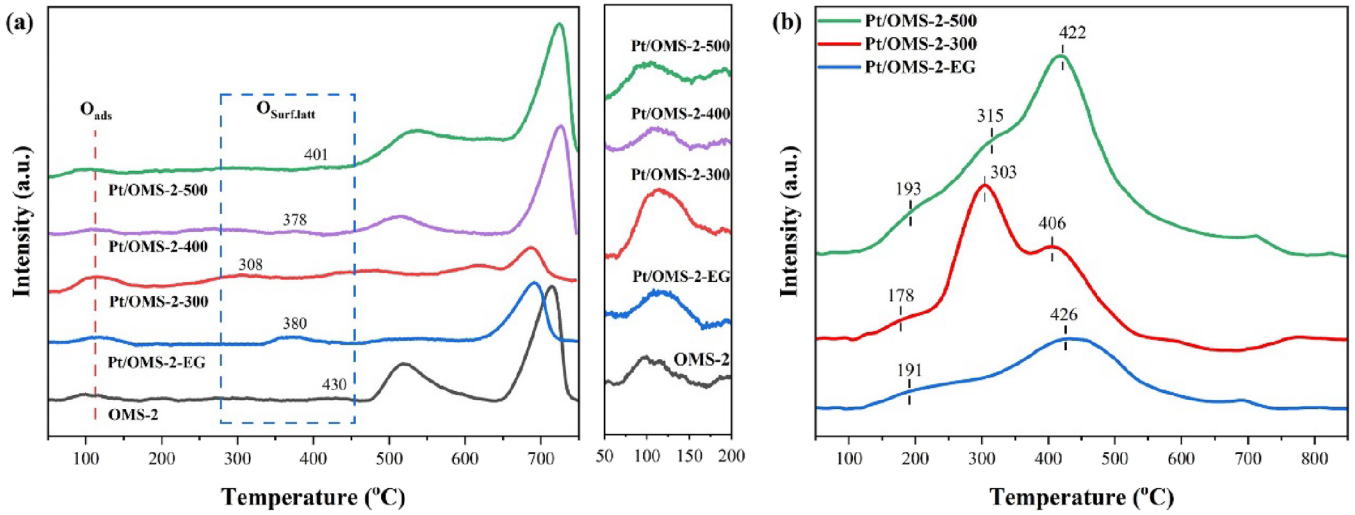

Figure 4. (a) O_2-TPD profiles of OMS-2 and Pt/OMS-2 samples and (b) toluene-TPD profiles of the Pt/OMS-2 samples.

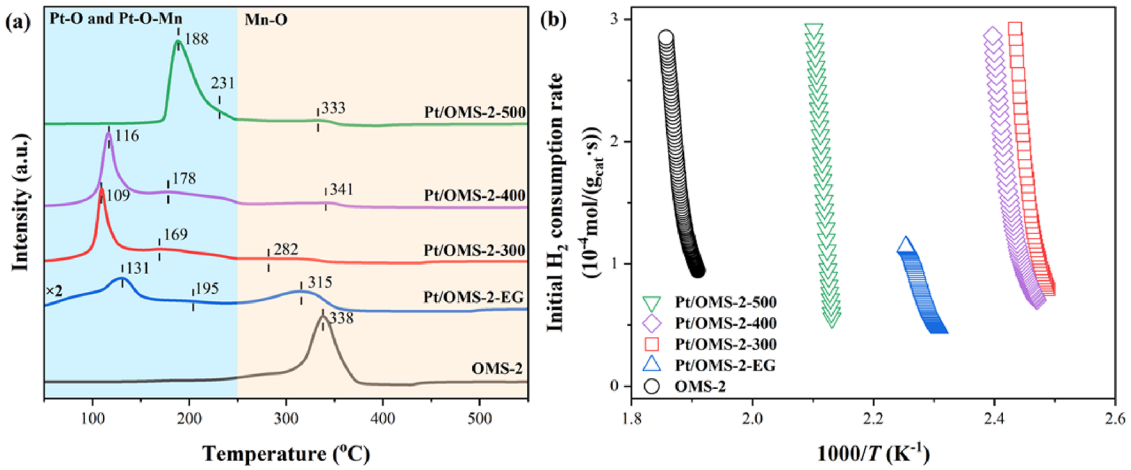

Figure 5. (a) H_2-TPR profiles and (b) initial H_2 consumption rate versus the inverse temperature of OMS-2 and Pt/OMS-2 samples.

peak appeared at 109−188 °C, which could be assigned to the reduction of Pt−O from the surface of Pt NPs and the Mn^{3+} or Mn^{4+} ions adjacent to the Pt NPs.[43] The reduction temperature of this peak depended on the calcined temperature, and it decreased first and increased further with the calcined temperature increasing, and the Pt/OMS-2-300 showed the lowest reduction temperature at 109 °C. The initial H_2 consumption rate (where less than 25% oxygen for the first reduction peak of the sample is removed) was put forward to represent the low-temperature reducibility.[44] Figure 5b shows that the initial H_2 consumption rate followed the order of Pt/OMS-2-300 > Pt/OMS-2-400 > Pt/OMS-2-EG > Pt/OMS-2-500 > OMS-2, which was well consistent with the order of O_{ads} content and catalytic activity (shown below). It could be inferred that the excellent low-temperature reducibility of Pt/OMS-2-300 could benefit toluene combustion. It should be noted that low H_2 consumption of Pt/OMS-2-EG was observed, which might be due to the relatively lower average valence of Pt and Mn species as well as the weak support−metal interaction (Table 2). As calcination temperature increased to 500 °C, the first reduction peak shifted by around 70 °C toward a high temperature, indicating that too strong SMSIs in Pt/OMS-2-500 would partially hinder the reactivity of surface oxygen species and make them difficult to reduce by H_2. The above results demonstrated that the strength of the SMSI could be tuned by controlling the calcination temperature and much more SSOVs in the Pt^{2+}−O_v−$Mn^{\delta+}$ structure were formed at the interface of Pt/OMS-2-300 with a moderate strength of the SMSI, which could optimize the oxygen species and improve the lattice oxygen mobility.

3.3. Catalytic Activity. The catalytic combustion curves of toluene over OMS-2 and Pt/OMS-2 catalysts are shown in Figure 6a. T_{90} (at which a toluene conversion of 90% was achieved) on all catalysts was also determined and is listed in Table 1 to better compare. Compared with pure OMS-2 samples, all Pt/OMS-2 catalysts exhibited much better toluene combustion activities, suggesting that Pt sites or the Pt−MnO_2 interface was more efficient than Mn-O sites. In addition, Pt/OMS-2-IMP with the same loading of Pt synthesized by the conventional wet impregnation method was used as a reference sample. The results showed that the OMS-2-supported Pt NPs prepared by the ethylene glycol reduction method still performed better than Pt/OMS-2-IMP. For the samples treated at different temperatures, Pt/OMS-2-300 showed the best catalytic oxidation activity for toluene with a much lower T_{90} of 162 °C comparing to Pt/OMS-2 catalysts calcined at lower or higher temperatures. Similar results were obtained

https://doi.org/10.1021/acsami.2c16923
ACS Appl. Mater. Interfaces 2022, 14, 56790−56800

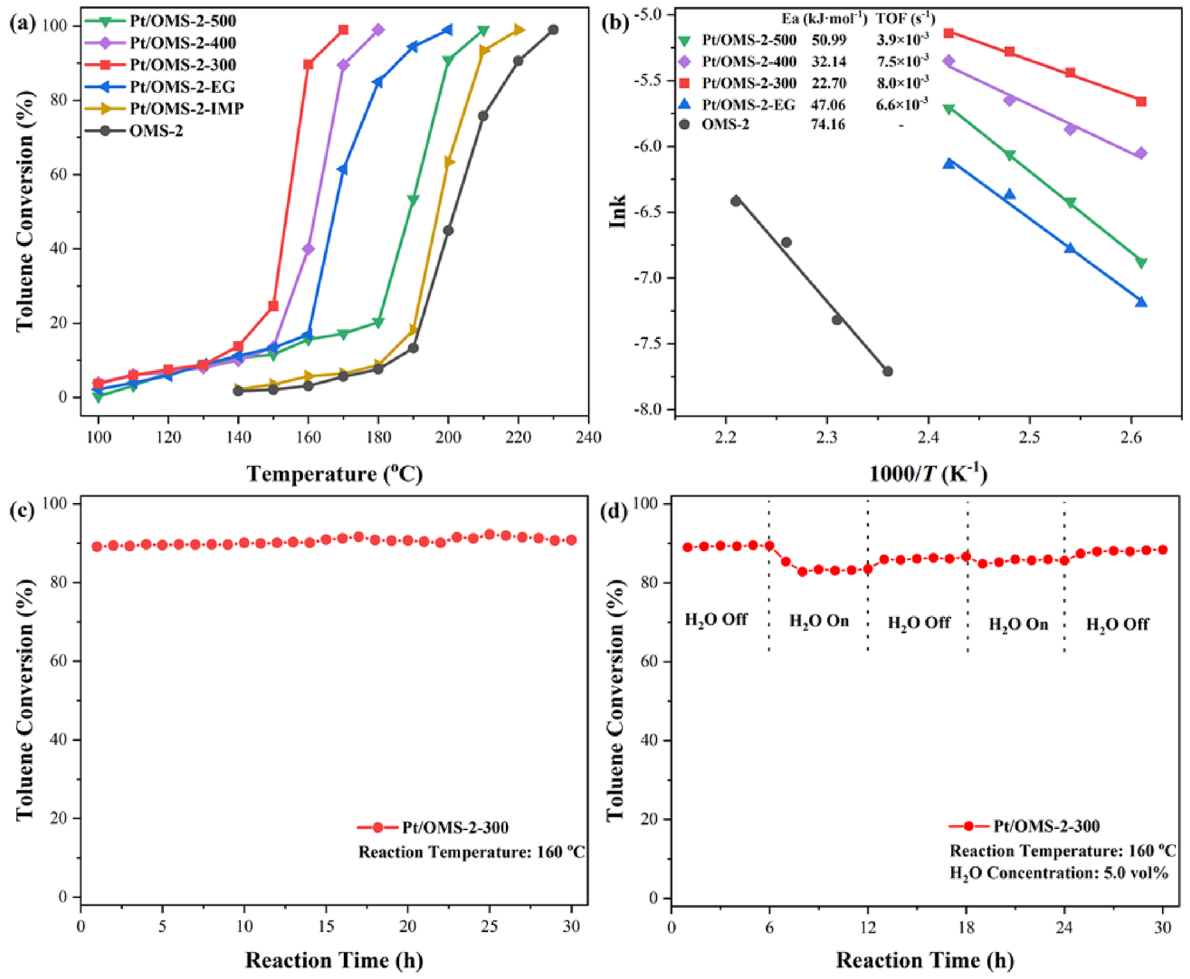

Figure 6. (a) Conversion of toluene over different catalysts. Catalyst amount: 100 mg. Toluene concentration: 1000 ppm. WHSV: 30,000 mL·g^{-1}·h^{-1}. (b) Arrhenius plots for the oxidation of toluene over different catalysts. (c) Toluene conversion over the Pt/OMS-2-160 catalyst at 160 °C. (d) Effect of water vapor on toluene conversion at 160 °C over Pt/OMS-2-300.

when measuring the CO_2 yield (Figure S4a). Compared with other studies for the catalytic oxidation of toluene summarized in Table S2, Pt/OMS-2-300 also showed excellent activity at a similar Pt loading. According to the previous report, the excellent catalytic performance could be obtained when the particle size of Pt NPs was controlled at approximately2 nm.[45] In this work, 2 nm Pt catalysts also showed significant catalytic activity for toluene oxidation.

Moreover, the apparent activation energy (E_a) was calculated using the Arrhenius equation at a low conversion rate for toluene oxidation (Figure 6b).[46] The order of E_a was Pt/OMS-2-300 (22.70 kJ·mol^{-1}) < Pt/OMS-2-400 (32.14 kJ·mol^{-1}) < Pt/OMS-2-EG (47.06 kJ·mol^{-1}) < Pt/OMS-2-500 (50.99 kJ·mol^{-1}) < OMS-2 (74.16 kJ·mol^{-1}). The lower values indicated the lower energy barrier for the oxidation of toluene on Pt/OMS-2-300, matching well with the activity results. The turnover frequency (TOF) values of Pt on these Pt-based catalysts were also calculated and are listed in Table 1.[32] The TOF_{Pt} values followed the sequence of Pt/OMS-2-300 > Pt/OMS-2-400 > Pt/OMS-2-EG > Pt/OMS-2-500. Notably, the Pt/OMS-2-300 exhibited the highest TOF_{Pt} value (8.0×10^{-3} s^{-1}). It could be inferred that the Pt/OMS-2-300 showed excellent low-temperature activity, indicating its good applying potential. After the toluene reaction, Pt/OMS-2-EG and Pt/OMS-2-300 samples were characterized by TEM and XPS as shown in Figures S5 and S6, and the particle size and chemical state of Pt are summarized in Table S3. It was found that the proportion of Pt^0 on Pt/OMS-2-EG decreased significantly and Pt agglomerated obviously. However, the surface chemical state and particle size of Pt in Pt/OMS-2-300 remained relatively stable, implying that the existence of the SMSI between the Pt species and OMS-2 support could improve the stability of Pt species.[47,48] Combined with the results of XPS, H_2-TPR, O_2-TPD, and toluene TPD, it could be concluded that the moderate strength of the SMSI on Pt/OMS-2 could facilitate the formation of more SSOVs (Pt^{2+}−O_v−$Mn^{\delta+}$) and thus enhance the reactivity/mobility of oxygen species, which could be one of the most important reasons for the best toluene combustion activity on Pt/OMS-2-300.

The thermal stability and water resistance ability of catalysts are also important indexes to evaluate the practical application prospect of Pt/OMS-2-300 for toluene elimination. Therefore, the thermal stability and water resistance of Pt/OMS-2-300 were investigated as illustrated in Figure 6c,d. The Pt/OMS-2-300 catalyst maintained a relatively high toluene conversion and good stability in the long-term (30 h) test at 160 °C. After the reaction, there existed just a little bit carbon deposition on the surface of the Pt/OMS-2-300 according to the TG-MS result (Figure S7). Moreover, after three cycles of the reaction, it still exhibited favorable catalytic activity (Figure S4b). In a

https://doi.org/10.1021/acsami.2c16923
ACS Appl. Mater. Interfaces 2022, 14, 56790−56800

real reaction, the existence of water vapor cannot be ignored. Toluene oxidation experiments of Pt/OMS-2-300 were conducted with 5 vol % water vapor, switching on/off alternatively at 160 °C for 30 h. The catalytic activity decreased when water vapor was inserted but recovered gradually when water vapor was switched off. The superior catalytic activity, stability, and H_2O resistance ability enabled Pt/OMS-2-300 a promising application prospect.

3.4. Reaction Mechanism. To further understand the pathway of toluene oxidation, in situ DRIFTS experiments were carried out, and the assignment of in situ DRIFTS bands is summarized in Table S4. As shown in Figure 7 and Table S4,

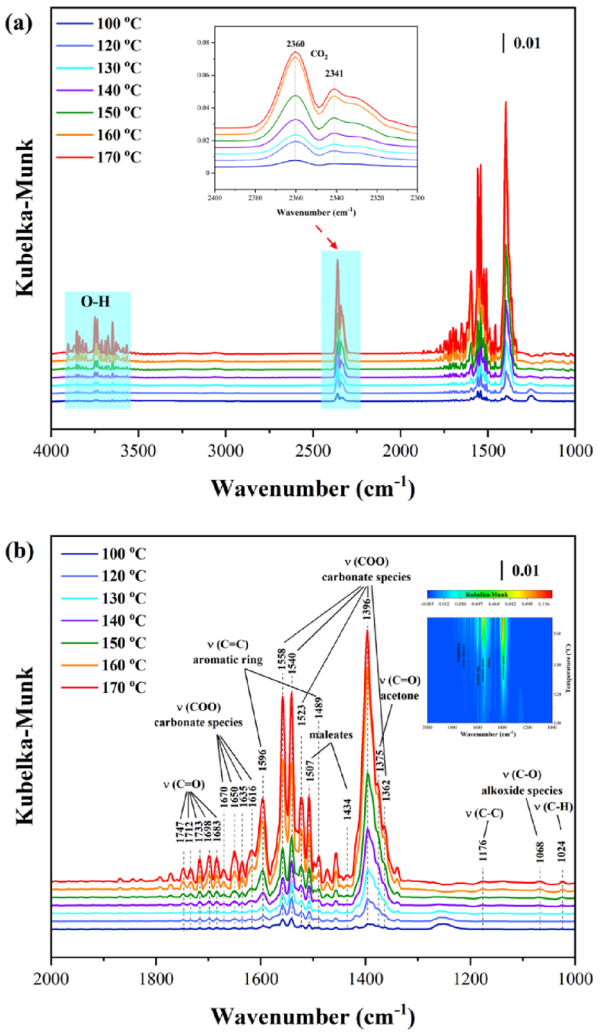

Figure 7. (a, b) In situ DRIFTS of toluene oxidation on the Pt/OMS-2-300 catalyst under different temperatures and corresponding contour color diagrams.

the vibration peak near 3700 cm^{-1} was attributed to ν(O−H).[49] The bands at 2341 and 2360 cm^{-1} were assigned to the CO_2 gas phase.[50] The bands of 1747, 1733, and 1698 cm^{-1} were attributed to ν(C═O) stretching vibrations of aldehydes.[32,51] For the vibrational bands of 1616−1635, 1650, 1669, 1520−1560, 1396, and 1362 cm^{-1}, they were assigned to the ν(C═O) stretching vibrations of aromatic acids and carboxylate groups, generally ascribed to the benzoate species and carbonate species.[52−54] Obviously, bands located at 1596 and 1489 cm^{-1} were assigned to skeleton ν(C═C) stretching vibration, indicating the existence of aromatic rings.[50] Notably, the characteristic bands at 1506 and 1434 cm^{-1} were derived from short-chain maleic anhydride, which were the key intermediates of an aromatic ring fracture.[55,56] The peak of 1068 cm^{-1} was attributed to the ν(C−O) stretching vibration of the alkoxide species.[51]

Figure S8 shows the in situ toluene adsorption at 100 °C as a function of time. Compared with the Pt/OMS-2-EG sample, Pt/OMS-2-300 and -500 showed a higher adsorption capacity for toluene, which might be due to the formation of the Pt−MnO_2 interface. This was well supported by the previous report in which $Pt^{\delta+}$ played an important role in the adsorption and activation of reactants for toluene oxidation.[57,58] For Pt/OMS-2-300, vibration peaks of an aromatic ring were detected even in the first 10 min, indicating that the adsorption of toluene was very fast. As time went on, the intensity of the aromatic ring became weaker, and the intensity of 1521−1560 cm^{-1} became stronger, indicating the accumulation of benzoate on the surface. Meanwhile, the band strengths of formate (1396 cm^{-1}) and acetate (1362 cm^{-1}) species were enhanced, which may be due to the further desorption of benzoate, and then partly oxidized to short-chain carbonate species by reactive oxygen species.[59] However, the vibration bands of benzoate were still strong even after adsorption for 50 min over the Pt/OMS-2-500 catalyst, indicating that Pt^{4+}−O−$Mn^{\delta+}$ had a stronger adsorption capacity for toluene compared to Pt^{2+}−O_v−$Mn^{\delta+}$. Such a strong adsorption might cause toluene and intermediates to accumulate on the surface of catalysts without further reaction with active oxygen species, thus resulting in a poisoning effect, which was consistent with the toluene TPD results.[7]

In situ DRIFTS of temperature-dependent toluene oxidation experiments over Pt/OMS-2-300 and Pt/OMS-2-EG were also conducted, and the obtained spectra were presented in the form of contour color diagrams (Figure 7 and Figure S9). A significant difference between two samples could be observed. The vibration peaks of the CO_2 gas phase and benzoate were detected at 120 °C on the Pt/OMS-2-300 sample. Meanwhile, the intensity of vibration bands of benzoate increased as the temperature was elevated, indicating the accumulation of benzoates. In this process, toluene was not completely oxidized and activated oxygen species participated in the catalytic reaction. It is worth noting that important aromatic ring fracture intermediates were detected at 160 °C, which were maleate species. The band at 1375 cm^{-1} was attributed to the acetone, implying the open-ring of toluene as well.[60] However, for Pt/OMS-2-EG, the characteristic vibration peak of CO_2 appeared at 140 °C, and the maleate species was observed over Pt/OMS-2-EG at 180 °C, indicating that, compared to Pt/OMS-2-EG, Pt/OMS-2-300 had obvious advantages in the open-ring step. Furthermore, Pt/OMS-2-300 was observed to easily oxidize short-chain carboxylate species based on the higher intensity in Figure 7b (representing shorter carboxylate species, particularly, the vibrational bands near 1362 and 1396 cm^{-1} were acetate). Under the same conditions, the intensity of the Pt/OMS-2-EG catalyst decreased obviously. These results proved that Pt/OMS-2-300 could better catalyze the combustion of toluene than Pt/OMS-2-EG. To better understand the reaction mechanism on Pt/OMS-2 catalysts, a reaction pathway was proposed and is shown in Figure 8. Here, $Pt^{\delta+}$ mainly played the role of adsorption of toluene. As for the adsorption/activation of oxygen species, SSOVs (Pt^{2+}−O_v−$Mn^{\delta+}$) at the Pt−MnO_2 interface could act as an oxygen

https://doi.org/10.1021/acsami.2c16923
ACS Appl. Mater. Interfaces 2022, 14, 56790−56800

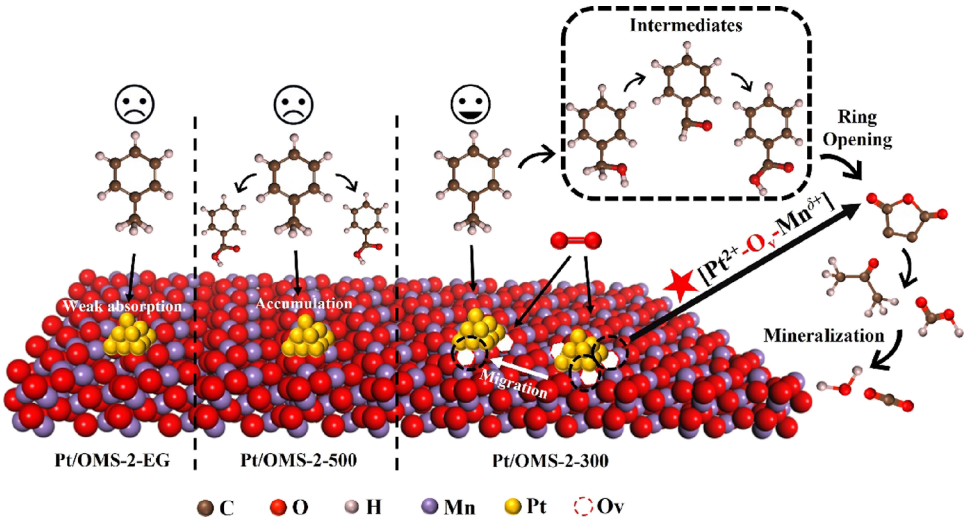

Figure 8. Proposed reaction pathway of toluene oxidation over Pt/OMS-2 catalysts.

"pump" to convert gaseous oxygen into surface-reactive oxygen species, which ultimately promoted the deep oxidation of toluene. Based on the results of in situ DRIFTS experiments and our group's previous report, it could be concluded that the toluene combustion on Pt/OMS-2 was proceeded by a Mars–van Krevelen (MvK) mechanism, and the degradation of toluene on Pt/OMS-2-300 catalyst mainly followed the process: toluene → benzyl alcohol → benzaldehyde → benzoate acid → maleates, short-chain carboxylates and aldehydes/ketones (acetone) → CO_2 and H_2O.[8,27,61]

4. CONCLUSIONS

In this work, the strong metal–support interaction (SMSI) between Pt and OMS-2 support is fine-tuned by controlling the calcination temperatures. The moderate strength of the SMSI on Pt/OMS-2-300 could promote the formation of more SSOVs (Pt^{2+}–O_v–$Mn^{\delta+}$), which then facilitated the adsorption, activation, and migration of oxygen species, thus significantly boosting the toluene oxidation activity on Pt/OMS-2-300. Pt/OMS-2-300 also exhibited good stability and resistance to H_2O. Moreover, the systematic mechanism study further revealed that the moderate strength of the SMSI on Pt/OMS-2-300 could better trigger the open-ring step in the toluene degradation process and hinder the accumulation of intermediates, which significantly benefited the complete oxidation of toluene. This work provides a simple but effective strategy to optimize the strength of SMSIs on Pt/MnO_2 catalysts for efficient catalytic combustion of toluene and advances the understanding of the reaction mechanism in toluene combustion to a significant step forward.

■ ASSOCIATED CONTENT

Supporting Information

The Supporting Information is available free of charge at https://pubs.acs.org/doi/10.1021/acsami.2c16923.

Detailed experimental procedures; characterization data of N_2 adsorption–desorption, TEM, HRTEM, Raman, XPS, TG-MS, and in situ DRIFTS; CO_2 yield and cycle of reactions; comparison of the toluene catalytic performance of Pt/OMS-2-300 with other literature reports; and assignment of IR bands of in situ DRIFTS (PDF)

■ AUTHOR INFORMATION

Corresponding Author

Haiqin Wan – *State Key Laboratory of Pollution Control and Resource Reuse, School of Environment, Jiangsu Key Laboratory of Vehicle Emissions Control, Nanjing University, Nanjing 210023, P.R. China;* orcid.org/0000-0003-0639-4576; Email: wanhq@nju.edu.cn

Authors

Lixin Zhang – *State Key Laboratory of Pollution Control and Resource Reuse, School of Environment, Jiangsu Key Laboratory of Vehicle Emissions Control, Nanjing University, Nanjing 210023, P.R. China*

Zhengxuan Zhu – *State Key Laboratory of Pollution Control and Resource Reuse, School of Environment, Jiangsu Key Laboratory of Vehicle Emissions Control, Nanjing University, Nanjing 210023, P.R. China*

Wei Tan – *State Key Laboratory of Pollution Control and Resource Reuse, School of Environment, Jiangsu Key Laboratory of Vehicle Emissions Control, Nanjing University, Nanjing 210023, P.R. China*

Jiawei Ji – *School of Chemistry and Chemical Engineering, Jiangsu Key Laboratory of Vehicle Emissions Control, Center of Modern Analysis, Nanjing University, Nanjing 210023, P.R. China*

Yandi Cai – *State Key Laboratory of Pollution Control and Resource Reuse, School of Environment, Jiangsu Key Laboratory of Vehicle Emissions Control, Nanjing University, Nanjing 210023, P.R. China*

Qing Tong – *School of Chemistry and Chemical Engineering, Jiangsu Key Laboratory of Vehicle Emissions Control, Center of Modern Analysis, Nanjing University, Nanjing 210023, P.R. China*

Yan Xiong – *School of Chemistry and Chemical Engineering, Southwest Petroleum University, Chengdu 610500, China;* orcid.org/0000-0002-4923-0179

Lin Dong – *State Key Laboratory of Pollution Control and Resource Reuse, School of Environment, Jiangsu Key Laboratory of Vehicle Emissions Control, Nanjing University, Nanjing 210023, P.R. China;* orcid.org/0000-0002-8393-6669

Complete contact information is available at:

https://doi.org/10.1021/acsami.2c16923
ACS Appl. Mater. Interfaces 2022, 14, 56790–56800

https://pubs.acs.org/10.1021/acsami.2c16923

Notes

The authors declare no competing financial interest.

■ ACKNOWLEDGMENTS

This work was supported by the financial support from the National Natural Science Foundation of China (nos. 21976082 and 22106067).

■ REFERENCES

(1) Wang, Y.; He, J.; Li, X.; Wang, M.; Zhou, Y.; Xiao, J.; Chen, D.; Lu, J. Low Temperature Combustion of VOCs with Enhanced Catalytic Activity Over MnO_2 Nanotubes Loaded with Pt and Ni-Fe Spinel. *ACS Appl. Mater. Interfaces* **2021**, *13*, 46830−46839.

(2) He, C.; Cheng, J.; Zhang, X.; Douthwaite, M.; Pattisson, S.; Hao, Z. Recent Advances in the Catalytic Oxidation of Volatile Organic Compounds: A Review Based on Pollutant Sorts and Sources. *Chem. Rev.* **2019**, *119*, 4471−4568.

(3) Zhang, H.; Zheng, X.; Xu, T.; Zhang, P. Atomically Dispersed Y or La on Birnessite-Type MnO_2 for the Catalytic Decomposition of Low-Concentration Toluene at Room Temperature. *ACS Appl. Mater. Interfaces* **2021**, *13*, 17532−17542.

(4) Guo, H.; Lee, S. C.; Chan, L. Y.; Li, W. M. Risk Assessment of Exposure to Volatile Organic Compounds in Different Indoor Environments. *Environ. Res.* **2004**, *94*, 57−66.

(5) Blasin-Aubé, V.; Belkouch, J.; Monceaux, L. General Study of Catalytic Oxidation of Various VOCs over $La_{0.8}Sr_{0.2}MnO_{3+x}$ Perovskite Catalyst—Influence of Mixture. *Appl. Catal., B* **2003**, *43*, 175−186.

(6) Bao, L.; Zhu, S.; Chen, Y.; Wang, Y.; Meng, W.; Xu, S.; Lin, Z.; Li, X.; Sun, M.; Guo, L. Anionic Defects Engineering of Co_3O_4 Catalyst for Toluene Oxidation. *Fuel* **2022**, *314*, 122774.

(7) Wei, X.; Li, K.; Zhang, X.; Tong, Q.; Ji, J.; Cai, Y.; Gao, B.; Zou, W.; Dong, L. CeO_2 Nanosheets with Anion-Induced Oxygen Vacancies for Promoting Photocatalytic Toluene Mineralization: Toluene Adsorption and Reactive Oxygen Species. *Appl. Catal., B* **2022**, *317*, 121694.

(8) Weng, X.; Shi, B.; Liu, A.; Sun, J.; Xiong, Y.; Wan, H.; Zheng, S.; Dong, L.; Chen, Y. W. Highly Dispersed Pd/modified-Al_2O_3 Catalyst on Complete Oxidation of Toluene: Role of Basic Sites and Mechanism Insight. *Appl. Surf. Sci.* **2019**, *497*, 143747.

(9) Wang, M.; Chen, D.; Li, N.; Xu, Q.; Li, H.; He, J.; Lu, J. Highly Efficient Catalysts of Bimetallic Pt-Ru Nanocrystals Supported on Ordered ZrO_2 Nanotube for Toluene Oxidation. *ACS Appl. Mater. Interfaces* **2020**, *12*, 13781−13789.

(10) Zhang, Z.; He, G.; Li, Y.; Zhang, C.; Ma, J.; He, H. Effect of Hydroxyl Groups on Metal Anchoring and Formaldehyde Oxidation Performance of Pt/Al_2O_3. *Environ. Sci. Technol.* **2022**, *56*, 10916−10924.

(11) Huang, Z.; Cao, S.; Yu, J.; Tang, X.; Guo, Y.; Guo, Y.; Wang, L.; Dai, S.; Zhan, W. Total Oxidation of Light Alkane over Phosphate-Modified Pt/CeO_2 Catalysts. *Environ. Sci. Technol.* **2022**, *56*, 9661−9671.

(12) Li, S.; Xu, Y.; Chen, Y.; Li, W.; Lin, L.; Li, M.; Deng, Y.; Wang, X.; Ge, B.; Yang, C.; Yao, S.; Xie, J.; Li, Y.; Liu, X.; Ma, D. Tuning the Selectivity of Catalytic Carbon Dioxide Hydrogenation over Iridium/Cerium Oxide Catalysts with a Strong Metal-Support Interaction. *Angew. Chem., Int. Ed. Engl.* **2017**, *56*, 10761−10765.

(13) Tauster, S. J.; Fung, S. C.; Garten, R. L. Strong Metal-Support Interactions. Group 8 Noble Metals Supported on TiO_2. *J. Am. Chem. Soc.* **1978**, 170−175.

(14) Wen, X.; Li, W.; Yan, J.; Wang, X.; Ren, E.; Shi, Z.; Li, J.; Ding, X.; Mo, S.; Mo, D. Strong Metal−Support Interaction in Pd/CeO_2 Promotes the Catalytic Activity of Ethyl Acetate Oxidation. *J. Phys. Chem. C* **2022**, *126*, 1450−1461.

(15) Xu, Z.; Mo, S.; Li, Y.; Zhang, Y.; Wu, J.; Fu, M.; Niu, X.; Hu, Y.; Ye, D. Pt/MnO_x for Toluene Mineralization via Ozonation Catalysis at Low Temperature: SMSI Optimization of Surface Oxygen Species. *Chemosphere* **2022**, *286*, 131754.

(16) Fujiwara, K.; Okuyama, K.; Pratsinis, S. E. Metal−Support Interactions in Catalysts for Environmental Remediation. *Environ. Sci.: Nano* **2017**, *4*, 2076−2092.

(17) Miao, S. J.; Deng, Y. Q. Study on Total Cooxidation of H_2 and CO over Au(Pt)/Co_3O_4 Catalysts under Oxygen-excessive Condition. *Chin. J. Catal.* **2001**, *22*, 461−464.

(18) Pereira-Hernández, X. I.; DeLaRiva, A.; Muravev, V.; Kunwar, D.; Xiong, H.; Sudduth, B.; Engelhard, M.; Kovarik, L.; Hensen, E. J. M.; Wang, Y.; Datye, A. K. Tuning Pt-CeO_2 Interactions by High-Temperature Vapor-Phase Synthesis for Improved Reducibility of Lattice Oxygen. *Nat. Commun.* **2019**, *10*, 1358.

(19) Wang, C.; Ma, J.; Liu, F.; He, H.; Zhang, R. The Effects of Mn^{2+} Precursors on the Structure and Ozone Decomposition Activity of Cryptomelane-Type Manganese Oxide (OMS-2) Catalysts. *J. Phys. Chem. C* **2015**, *119*, 23119−23126.

(20) Hu, J.; Gao, X.; Fan, Q.; Gao, X. Facial Controlled Synthesis of Pt/MnO_2 Catalysts with High Efficiency for VOCs Combustion. *RSC Adv.* **2021**, *11*, 16547−16556.

(21) Mo, S.; Zhang, Q.; Zhang, M.; Zhang, Q.; Li, J.; Fu, M.; Wu, J.; Chen, P.; Ye, D. Elucidating the Special Role of Strong Metal−Support Interactions in Pt/MnO_2 Catalysts for Total Toluene Oxidation. *Nanoscale Horiz.* **2019**, *4*, 1425−1433.

(22) Bi, F.; Zhang, X.; Xiang, S.; Wang, Y. Effect of Pd Loading on ZrO_2 Support Resulting from Pyrolysis of UiO-66: Application to CO Oxidation. *J. Colloid Interface Sci.* **2020**, *573*, 11−20.

(23) Schick, L.; González-Alfaro, V.; García, A.; López, J. M.; Morgan, D. J.; Agouram, S.; Taylor, S. H.; García, T.; Solsona, B. Supported Iridium Catalysts for the Total Oxidation of Short Chain Alkanes and Their Mixtures: Influence of the Support. *Chem. Eng. J.* **2021**, *417*, 127999.

(24) Wu, K.; Sun, Y.; Liu, J.; Xiong, J.; Wu, J.; Zhang, J.; Fu, M.; Chen, L.; Huang, H.; Ye, D. Nonthermal Plasma Catalysis for Toluene Decomposition over $BaTiO_3$-Based Catalysts by Ce Doping at A-Sites: The Role of Surface-Reactive Oxygen Species. *J. Hazard. Mater.* **2021**, *405*, 124156.

(25) Su, Z.; Yang, W.; Wang, C.; Xiong, S.; Cao, X.; Peng, Y.; Si, W.; Weng, Y.; Xue, M.; Li, J. Roles of Oxygen Vacancies in the Bulk and Surface of CeO_2 for Toluene Catalytic Combustion. *Environ. Sci. Technol.* **2020**, *54*, 12684−12692.

(26) Quinson, J.; Inaba, M.; Neumann, S.; Swane, A. A.; Bucher, J.; Simonsen, S. B.; Theil Kuhn, L.; Kirkensgaard, J. J. K.; Jensen, K. M. Ø.; Oezaslan, M.; Kunz, S.; Arenz, M. Investigating Particle Size Effects in Catalysis by Applying a Size-Controlled and Surfactant-Free Synthesis of Colloidal Nanoparticles in Alkaline Ethylene Glycol: Case Study of the Oxygen Reduction Reaction on Pt. *ACS Catal.* **2018**, *8*, 6627−6635.

(27) Zhang, Y.; Wu, C.; Wang, Z.; Ji, J.; Wan, H.; Zou, W.; Tong, Q.; Sun, J.; Dong, L.; Chen, Y. W. Enhanced Low-Temperature Catalytic Performance for Toluene Combustion of CeO_2-Supported Pt-Ir Alloy Catalysts. *Appl. Surf. Sci.* **2022**, *580*, 152278.

(28) Fang, Y.; Li, H.; Zhang, Q.; Wang, C.; Xu, J.; Shen, H.; Yang, J.; Pan, C.; Zhu, Y.; Luo, Z.; Guo, Y. Oxygen Vacancy-Governed Opposite Catalytic Performance for C_3H_6 and C_3H_8 Combustion: The Effect of the Pt Electronic Structure and Chemisorbed Oxygen Species. *Environ. Sci. Technol.* **2022**, *56*, 3245−3257.

(29) Wang, F.; Dai, H.; Deng, J.; Bai, G.; Ji, K.; Liu, Y. Manganese Oxides with Rod-, Wire-, Tube-, and Flower-like Morphologies: Highly Effective Catalysts for the Removal of Toluene. *Environ. Sci. Technol.* **2012**, *46*, 4034−4041.

(30) Liu, L.; Song, Y.; Fu, Z.; Ye, Q.; Cheng, S.; Kang, T.; Dai, H. Effect of Preparation Method on the Surface Characteristics and Activity of the Pd/OMS-2 Catalysts for the Oxidation of Carbon Monoxide, Toluene, and Ethyl Acetate. *Appl. Surf. Sci.* **2017**, *396*, 599−608.

(31) Hou, J.; Li, Y.; Liu, L.; Ren, L.; Zhao, X. Effect of Giant Oxygen Vacancy Defects on the Catalytic Oxidation of OMS-2 Nanorods. *J. Mater. Chem. A* **2013**, *1*, 6736−6741.

(32) Mo, S.; Li, J.; Liao, R.; Peng, P.; Li, J.; Wu, J.; Fu, M.; Liao, L.; Shen, T.; Xie, Q.; Ye, D. Unraveling the Decisive Role of Surface CeO_2 Nanoparticles in the Pt-CeO_2/MnO_2 Hetero-Catalysts for Boosting Toluene Oxidation: Synergistic Effect of Surface Decorated and Intrinsic O-vacancies. *Chem. Eng. J.* **2021**, *418*, 129939.
(33) Zhang, Y.; Zhang, X.; Yang, P.; Gao, M.; Feng, J.; Li, D. In Situ Topologically Induced PtZn Alloy @ $ZnTiO_x$ and the Synergistic Effect on Glycerol Oxidation. *Appl. Catal., B* **2021**, *298*, 120634.
(34) Prabhuram, J.; Zhao, T. S.; Wong, C. W.; Guo, J. W. Synthesis and Physical/Electrochemical Characterization of Pt/C Nanocatalyst for Polymer Electrolyte Fuel Cells. *J. Power Sources* **2004**, *134*, 1−6.
(35) Tan, W.; Xie, S.; Cai, Y.; Wang, M.; Yu, S.; Low, K. B.; Li, Y.; Ma, L.; Ehrlich, S. N.; Gao, F.; Dong, L.; Liu, F. Transformation of Highly Stable Pt Single Sites on Defect Engineered Ceria into Robust Pt Clusters for Vehicle Emission Control. *Environ. Sci. Technol.* **2021**, *55*, 12607−12618.
(36) Iltona, E. S.; Post, J. E.; Heaneyc, P. J.; Ling, F. T.; Kerisit, S. N. Pacific XPS Determination of Mn Oxidation States in Mn (hydr)oxides. *Appl. Surf. Sci.* **2016**, *366*, 475−485.
(37) Li, D.; Yu, Q.; Li, S.-S.; Wan, H.-Q.; Liu, L.-J.; Qi, L.; Liu, B.; Gao, F.; Dong, L.; Chen, Y. The Remarkable Enhancement of CO-Pretreated CuO-Mn_2O_3/gamma-Al_2O_3 Supported Catalyst for the Reduction of NO with CO: the Formation of Surface Synergetic Oxygen Vacancy. *Chem. − Eur. J.* **2011**, *17*, 5668−5679.
(38) Pei, W.; Liu, Y.; Deng, J.; Zhang, K.; Hou, Z.; Zhao, X.; Dai, H. Partially Embedding Pt Nanoparticles in the Skeleton of 3DOM Mn_2O_3: An Effective Strategy for Enhancing Catalytic Stability in Toluene Combustion. *Appl. Catal., B* **2019**, *256*, 117814.
(39) Feng, Y.; Wang, C.; Wang, C.; Huang, H.; Hsi, H. C.; Duan, E.; Liu, Y.; Guo, G.; Dai, H.; Deng, J. Catalytic Stability Enhancement for Pollutant Removal via Balancing Lattice Oxygen Mobility and VOCs Adsorption. *J. Hazard. Mater.* **2022**, *424*, 127337.
(40) Chen, L.; Chen, P.; Wang, H.; Cui, W.; Sheng, J.; Li, J.; Zhang, Y.; Zhou, Y.; Dong, F. Surface Lattice Oxygen Activation on $Sr_2Sb_2O_7$ Enhances the Photocatalytic Mineralization of Toluene: from Reactant Activation, Intermediate Conversion to Product Desorption. *ACS Appl. Mater. Interfaces* **2021**, *13*, 5153−5164.
(41) Gan, T.; Chu, X.; Qi, H.; Zhang, W.; Zou, Y.; Yan, W.; Liu, G. Pt/Al_2O_3 with Ultralow Pt-Loading Catalyze Toluene Oxidation: Promotional Synergistic Effect of Pt Nanoparticles and Al_2O_3 Support. *Appl. Catal., B* **2019**, *257*, 117943.
(42) Yu, X.; He, J.; Wang, D.; Hu, Y.; Tian, H.; He, Z. Facile Controlled Synthesis of Pt/MnO_2 Nanostructured Catalysts and Their Catalytic Performance for Oxidative Decomposition of Formaldehyde. *J. Phys. Chem. C* **2011**, *116*, 851−860.
(43) Zhang, N.; Li, L.; Wu, R.; Song, L.; Zheng, L.; Zhang, G.; He, H. Activity Enhancement of Pt/MnO_x Catalyst by Novel β-MnO_2 for Low-Temperature CO Oxidation: Study of the CO−O_2 Competitive Adsorption and Active Oxygen Species. *Catal. Sci. Technol.* **2019**, *9*, 347−354.
(44) Chen, K.; Xie, S.; Bell, A. T.; Iglesia, E. Structure and Properties of Oxidative Dehydrogenation Catalysts Based on MoO_3/Al_2O_3. *J. Catal.* **2001**, *198*, 232−242.
(45) Peng, R.; Li, S.; Sun, X.; Ren, Q.; Chen, L.; Fu, M.; Wu, J.; Ye, D. Size Effect of Pt Nanoparticles on the Catalytic Oxidation of Toluene over Pt/CeO_2 Catalysts. *Appl. Catal., B* **2018**, *220*, 462−470.
(46) Xiao, M.; Yu, X.; Guo, Y.; Ge, M. Boosting Toluene Combustion by Tuning Electronic Metal−Support Interactions in In Situ Grown Pt@Co_3O_4 Catalysts. *Environ. Sci. Technol.* **2022**, *56*, 1376−1385.
(47) Liu, A.; Liu, L.; Cao, Y.; Wang, J.; Si, R.; Gao, F.; Dong, L. Controlling Dynamic Structural Transformation of Atomically Dispersed CuO_x Species and Influence on Their Catalytic Performances. *ACS Catal.* **2019**, *9*, 9840−9851.
(48) Jiang, Z.; Jing, M.; Feng, X.; Xiong, J.; He, C.; Douthwaite, M.; Zheng, L.; Song, W.; Liu, J.; Qu, Z. Stabilizing Platinum Atoms on CeO_2 Oxygen Vacancies by Metal-Support Interaction Induced Interface Distortion: Mechanism and Application. *Appl. Catal., B* **2020**, *278*, 119304.
(49) Chen, C.; Kosari, M.; He, C.; Ma, M.; Tian, M.; Jiang, Z.; Albilali, R. Realizing Toluene Deep Mineralization by Coupling Nonthermal Plasma and Nitrogen-Enriched Hollow Hybrid Carbon. *ACS Appl. Mater. Interfaces* **2022**, *14*, 990−1001.
(50) Sun, H.; Liu, Z.; Chen, S.; Quan, X. The Role of Lattice Oxygen on the Activity and Selectivity of the OMS-2 Catalyst for the Total Oxidation of Toluene. *Chem. Eng. J.* **2015**, *270*, 58−65.
(51) Shen, Y.; Deng, J.; Impeng, S.; Li, S.; Yan, T.; Zhang, J.; Shi, L.; Zhang, D. Boosting Toluene Combustion by Engineering Co-O Strength in Cobalt Oxide Catalysts. *Environ. Sci. Technol.* **2020**, *54*, 10342−10350.
(52) Lu, A.; Sun, H.; Zhang, N.; Che, L.; Shan, S.; Luo, J.; Zheng, J.; Yang, L.; Peng, D. L.; Zhong, C. J.; Chen, B. Surface Partial-Charge-Tuned Enhancement of Catalytic Activity of Platinum Nanocatalysts for Toluene Oxidation. *ACS Catal.* **2019**, *9*, 7431−7442.
(53) Coronado, J. M.; Kataoka, S.; Tejedor-Tejedor, I.; Anderson, M. A. Dynamic Phenomena during the Photocatalytic Oxidation of Ethanol and Acetone over Nanocrystalline TiO_2: Simultaneous FTIR Analysis of Gas and Surface Species. *J. Catal.* **2003**, *219*, 219−230.
(54) Mo, S.; Zhang, Q.; Sun, Y.; Zhang, M.; Li, J.; Ren, Q.; Fu, M.; Wu, J.; Chen, L.; Ye, D. Gaseous CO and Toluene Co-Oxidation over Monolithic Core−Shell Co_3O_4-based Hetero-Structured Catalysts. *J. Mater. Chem. A* **2019**, *7*, 16197−16210.
(55) Yang, W.; Peng, Y.; Wang, Y.; Wang, Y.; Liu, H.; Su, Z.'a.; Yang, W.; Chen, J.; Si, W.; Li, J. Controllable Redox-Induced In-Situ Growth of MnO_2 over Mn_2O_3 for Toluene Oxidation: Active Heterostructure Interfaces. *Appl. Catal., B* **2020**, *278*, 119279.
(56) Huang, H.; Gu, Y.; Zhao, J.; Wang, X. Catalytic Combustion of Chlorobenzene over VO /CeO_2 Catalysts. *J. Catal.* **2015**, *326*, 54−68.
(57) Wang, Q.; Li, Y.; Serrano-Lotina, A.; Han, W.; Portela, R.; Wang, R.; Bañares, M. A.; Yeung, K. L. Operando Investigation of Toluene Oxidation over 1D Pt@CeO_2 Derived from Pt Cluster-Containing MOF. *J. Am. Chem. Soc.* **2021**, *143*, 196−205.
(58) Nie, L.; Mei, D.; Xiong, H.; Peng, B.; Ren, Z.; Hernandez, X. I. P.; DeLaRiva, A.; Wang, M.; Engelhard, M. H.; Kovarik, L.; Datye, A. K.; Wang, Y. Activation of Surface Lattice Oxygen in Single-atom Pt/CeO_2 for Low-Temperature CO Oxidation. *Science* **2017**, *358*, 1419−1423.
(59) Rong, S.; Zhang, P.; Yang, Y.; Zhu, L.; Wang, J.; Liu, F. MnO_2 Framework for Instantaneous Mineralization of Carcinogenic Airborne Formaldehyde at Room Temperature. *ACS Catal.* **2017**, *7*, 1057−1067.
(60) Wang, Z.; Yang, H.; Liu, R.; Xie, S.; Liu, Y.; Dai, H.; Huang, H.; Deng, J. Probing Toluene Catalytic Removal Mechanism over Supported Pt Nano- and Single-Atom-Catalyst. *J. Hazard. Mater.* **2020**, *392*, 122258.
(61) Wang, Z.; Zhang, L.; Ji, J.; Wu, Y.; Cai, Y.; Yao, X.; Gu, X.; Xiong, Y.; Wan, H.; Dong, L.; Chen, Y. W. Catalytic Enhancement of Small Sizes of CeO_2 Additives on Ir/Al_2O_3 for Toluene Oxidation. *Appl. Surf. Sci.* **2022**, *571*, 151200.

https://doi.org/10.1021/acsami.2c16923
ACS Appl. Mater. Interfaces 2022, 14, 56790−56800